Thin Solid Films 516 (2008) 8768–8773

Contents lists available at ScienceDirect

Thin Solid Films

journal homepage: www.elsevier.com/locate/tsf

Superconducting niobium nitride films deposited by unbalanced magnetron sputtering

J.J. Olaya [a], L. Huerta [b], S.E. Rodil [b,*], R. Escamilla [b]

[a] Departamento de Ingeniería Mecánica y Mecatrónica, Universidad Nacional de Colombia, Ciudad Universitaria, Carrera 30 Número 45-03, Bogotá, Colombia
[b] Instituto de Investigaciones en Materiales, Universidad Nacional Autónoma de México, Circuito exterior s/n, CU Coyoacan, México D.F. 04510, Mexico

ARTICLE INFO

Article history:
Received 12 December 2007
Received in revised form 29 May 2008
Accepted 20 June 2008
Available online 25 June 2008

PACS:
79.20.2m
61.10.2i
74.76.2w
82.80.Pv

Keywords:
Magnetron sputtering
Superconducting films
Nitride
Niobium nitride
Electron spectroscopy

ABSTRACT

Niobium nitride (NbN) thin films were deposited under different configurations of the magnetic field using a magnetron sputtering system. The magnetic field configuration varied from balanced to unbalanced leading to different growth conditions and film properties. The aim of the paper was to identify correlations between deposition conditions, film properties and the electrical properties, specially the superconductive critical temperature (T_C).

The results suggested that there is a critical deposition condition, having an optimum ion–atom arrival ratio that promotes a well ordered and textured nanocrystalline structure (cubic phase) with the minimum residual stress and only under this condition a high critical temperature (16K) was obtained. Lower T_C values around 12K were obtained for the NbN samples having a lower degree of structural perfection and texture, and a larger fraction of intergranular voids. On the other hand, analysis of valence-band spectra showed that the contribution of the Nb 4d states remained essentially constant while the higher T_C was correlated to a higher contribution of the N 2p states.

1. Introduction

Niobium nitrides (NbN_x) are potential candidates for use in various cryogenic devices like high resolution X-ray [1] and electromagnetic radiation detectors ranging from millimeter wavelength to visible light [2]. Their relatively high critical superconducting temperature allows them to be used as diffusion barrier in Josephson junctions and as coatings for super conductive cables [3,4]. Also, their high hardness [5,6], their remarkable corrosion resistance [7], as well as their good chemical stability at high temperature (1000 °C) [8], make NbN_x a useful coating as a hard superconducting material to be used in extreme conditions [9]. The initial results about superconductivity in NbN films deposited by D.C. magnetron sputtering showed that a wide range of critical fields, superconductivity critical temperatures and resistivities could be obtained by changing the various deposition parameters, such as, substrate temperature, nitrogen partial pressure, cathode–substrate distance, etc [10,11]. Moreover, small changes in sputtering conditions resulted in unexpected changes in T_Cs and these results were interpreted in terms of the variations induced in the film structure, such as, O or C contaminants, metal vacancies, grain size, intergrain size, etc. However, a clear explanation of the decreasing T_C mechanism is still lacking. Recently, there has been a re-born interest in NbN thin films for advanced applications, such as, phonon-cooled hot electron bolometers, superconducting single-photon detectors, superconductivity cavities, barrier layers or to improve superconductor–semiconductor structures for electronic devices [10,12–15]. Therefore, the optimization of the structural properties of NbN films which usually leads to higher critical temperatures is a demanding task [16]. On the other hand, in the last decades magnetron sputtering systems have developed into better systems, including unbalanced magnetron sputtering and the use of pulse D.C. sources [17,18], which have shown to be effective systems to control the ion bombardment during deposition and thus, the microstructural film properties. One of the important advantages of unbalanced magnetron sputtering is the possibility to obtain high crystalline samples at lower deposition temperatures, which is a very important issue for the deposition of films on substrates which cannot stand high temperatures. Therefore, it is necessary to study the effect of the sputtering parameters on the superconducting and electrical properties of the UBM-deposited NbN films.

In this study, we report the effect of the magnetic field configuration of a magnetron system on the superconducting critical temperature (T_C) of NbN films and correlate the T_Cs with the microstructural, electronic and compositional properties. The different magnetic field configurations induced a higher ion bombardment

* Corresponding author.
E-mail address: ser42@iim.unam.mx (S.E. Rodil).

0040-6090/$ – see front matter © 2008 Elsevier B.V. All rights reserved.
doi:10.1016/j.tsf.2008.06.065

Table 1
Deposition conditions and results

Sample	K	V_p (V)	J_i/J_a	a-111 (nm)[a]	gz-002 (nm)	gz-111 (nm)	$T_{[002]}$	E (GPa)	H (GPa)	T_C (K)
NbN-BM	1	10.3	1.6	4.435	20	13.5	0.29	357.2	26	–
NbN-0	6.5	10.4	1.7	4.461	24.7	20	0.987	343.3	22.7	16
NbN-3	7.3	11.1	2	4.475	20	34	0.3	437	37.7	12.9
NbN-5	9.1	11.4	2.6	4.478	14.7	22.3	0.11	435	38.2	12.6

K is the unbalance parameter, V_p is the plasma potential, J_i/J_a is the ion–atom flux ratio, a-111 is the lattice parameter estimated from the XRD (111) peak position, gz is the grain size, $T_{[002]}$ is the relative texture factor, E is the elastic modulus, H is the hardness and T_C is the superconductive critical temperature.
[a] a-200 lattice parameter were ~4.412 nm for the samples deposited with UBM.

on the growing films, leading to more compact and highly texture crystalline structures, and consequently we observed variations in the T_Cs.

2. Experimental details

The NbN films were produced using an unbalanced magnetron sputtering cathode from Teer Coatings Ltd. This system offers the possibility of varying the magnetic field configuration of the magnetron, by changing the vertical distance between the permanent magnets and the target [19]. This variation leads to different degrees of unbalancing (K), which are defined as the ratio of the Z magnetic field components from the central to peripheral magnets on the target surface, where K equals the unity for a perfect balanced magnetron and becomes larger than 1 for unbalanced systems [20].

$$K = \frac{\int B_{\text{central}} dZ_{\text{central}}}{\int B_{\text{external}} dZ_{\text{external}}}$$

Three films were deposited using the Teer UBM system changing K from 6.5 to 9.1. For comparison, we also deposited NbN samples using a conventional or balanced magnetron system (BM), equivalent to $K=1$.

The coatings were deposited from a high purity Nb target of 101mm in diameter (99.95%), in Ar+N_2 (both of 99.99% purity) atmospheres. The base pressure in the chamber was less than 6×10^{-4} Pa. The deposition conditions were: pressure (0.9 Pa), flow-rate ratio Ar/N_2 (7) and power (200W). The substrate temperature was fixed at 380 °C, which for NbN corresponds to a homologous temperature of 0.158 (homologous temperature is the ratio between the substrate temperature and the melting temperature of the material). The deposition conditions used were previously optimized to obtain a stoichiometric (1:1) hard metal nitride film under fixed K conditions, and the variation of the composition and microstructural properties with K were later studied. The deposition time was adjusted to set the thickness of all coatings to about 1.8μm. The substrates were crystalline Si (111) containing the native oxide and were grounded without application of any external bias. The thickness was measured with a stylus profilometer DEKTAK IIA.

In order to determine the ion bombardment parameters, the plasma potential (V_p) was determined from the current–voltage characteristic of a cylindrical probe and the ion current densities (J_i) were measured using a 0.125mm^2 planar probe at a direct current, D.C. bias of − 100V. All the measurements were made at the deposition conditions mentioned above, placing the probes at 5cm from the target and radially in the centre of it [19].

Phase identification of the films was performed using an X-ray diffractometer (XRD), Siemens D5000 with Cu-Kα radiation and Ni filter. Intensities were measured in steps of 0.02° for 14s in the 2θ range from 30 to 120, at room temperature. The grain size, D, was calculated from the full width half maximum of the appropriate peaks using the Debye–Scheerrer equation and the lattice parameter, a, was estimated from the peak position [19,21].

The superconducting transition temperature was determined with a closed-cycle helium refrigerator by measuring the resistance vs. temperature (R vs. T) characteristic by the standard four-probe technique, from 250K to 14K. The reported superconducting transition temperature corresponds to the temperature value at which the resistance goes to zero.

The chemical analysis was carried out by X-ray photoelectron spectroscopy (XPS). This analysis was performed using an ultra-high vacuum system of VG Microtech ESCA2000 Multilab, with a Mg Kα X-ray source ($h\nu$=253.6eV) and CLAM4 multichannel detector analyser. The XPS error is based considering a detection limit estimated to be ~ 1% and proper propagation of uncertainties.

3. Results

The sample names and results of the plasma characterization for the UBM and the BM systems are included in Table 1, more details can be found in references [19,21,22]. The ion–atom condensing flux ratio, J_i/J_a was estimated from the plasma characterization results, the deposition rate and the volumetric film density of bulk NbN (8.43g/cm^3) according to [23]. In Table 1, it might be observed that as the degree of unbalance, K increased, the ratio J_i/J_a increased from 1.6 to 2.6, while the ion energy, which is proportional to the plasma potential, remained around 10–11eV.

Fig. 1 shows the normalized sheet resistance "$r=R(T)$ / R(280K)" versus temperature curve for the NbN films deposited with the balanced and unbalanced magnetron systems. The resistance at 280K, R_{280} of the films varied between 210μΩ to 175μΩ for NbN-0, NbN-3, NbN-5 and NbN-BM. From the trends in Fig. 1, one might see that for NbN-3, NbN-5 and NbN-BM thin films, the normalized resistance decreased monotonically as the temperature decreased exhibiting a metallic-like behavior (i.e., the equivalent to a positive temperature coefficient of resistivity, TCR) with a residual resistance ratio (RRR) given by the ratio R_{280}/R_{20} between 1.11 and 1.18. On the other hand, for the NbN-0 a decreasing slope with increasing T was observed, suggesting a semiconductor-like behavior (negative TCR) with a RRR values slightly lower (0.93). However, within the experimental error, we could say that all the RRR values are close to unity, similar to previous reported values for NbN films [10,24–27].

From Fig. 1, it might also be seen that, except for the NbN-BM, the other NbN thin films showed a clear transition to the superconducting state within the range obtained by the cryopump (14K) system. The T_C for the NbN-0 was obtained as the temperature value at which the resistance is zero and for the NbN-3 and NbN-5 samples, an

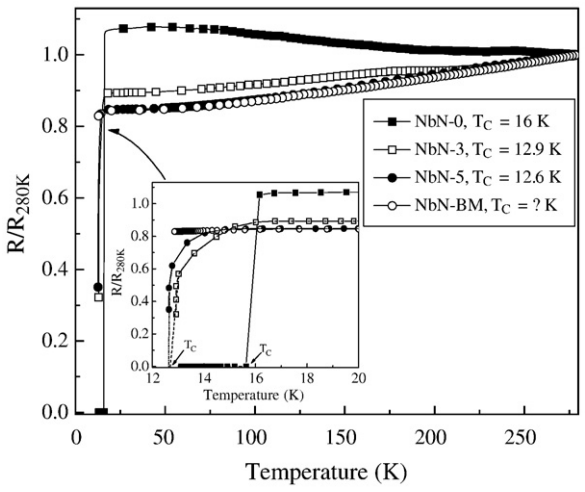

Fig. 1. Normalized resistance versus temperature of NbN films deposited with the balanced and unbalanced magnetron. The inset shows the superconductive transition and the point at which the T_C was defined.

extrapolation of the r vs. T curve was used to estimate the zero resistance temperature, as shown in the inset of Fig. 1. As observed, no T_C can be obtained for the NbN-BM sample within the experimental range. The maximum T_C corresponded to the NbN-0 (16K) while the values for NbN-3 and NbN-5 films were 12.9 and 12.6K, respectively. The T_C of the NbN-0 film compared well with the highest T_C reported in literature for NbN films (T_C=16.9K [28], T_C=17.3 K [29]).

Fig. 2 shows the X-ray diffraction patterns for the NbN films deposited with both the BM and UBM systems. The structural analysis indicated that all samples displayed the NbN (ICDD No. 71-0162) phase with negligible content of the metallic Nb (ICDD No. 35-0789) [30]. Analysis of the full spectra (20–130°) were done to confirm that the main diffraction peaks observed are those related to the (111) and (002) orientations of the face-centred cubic, FCC phase of δ-NbN, together with a small peak at $2\theta \approx 118°$ which also corresponds to the (422) cubic δ-NbN phase, which confirmed the δ-phase. The region around $2\theta \approx 60–70°$, which is associated with δ′-NbN hexagonal phase (JCPDS No. 14-0547) is shown in the inset [30]. It might be seen that a considerable signal of the (2θ=62°) peak is only observed for the NbN-BM sample.

The spectra in Fig. 2 also shows that the intensity of the XRD peaks of the BM sample are much lower than that of the UBM-deposited samples, although the film thicknesses are similar. This difference is particularly clear comparing NbN-BM to the NbN-0 sample and might indicate the superior structural perfection (less defects, grain boundaries, etc) of the UBM samples. Moreover, it might be seen that the preferred orientation of the samples varied as a function of the unbalancing K factor. This variation can be estimated considering the [002] texture factor ($T_{[002]}$) defined as the ratio of the (002) intensity peak divided by the sum of the other peak intensities [31]. An estimation of this texture factor from standard XRD patterns corresponding to powder samples, i.e. randomly oriented samples, suggest that any value of $T_{[002]}$ larger than 0.4 is a clear indication of preferred [002] orientation. Both NbN-3 and BM samples showed a mixed [111]+[002] orientation ($T_{[002]}$ factors between 0.29 and 0.3, respectively), while the NbN-0 sample showed a preferred [002] orientation ($T_{[002]}$=0.99) and the NbN-5 a [111] orientation ($T_{[002]}$=0.11). These results indicated that the K factor is not sufficient to explain the variations in sample texture, an explanation for this variation have been given in previous papers in terms of a synergetic effect between the ion bombardment and the efficiency of N_2 dissociation [21,22,32]. The lattice parameter and the grain size as a function of the unbalance factor K, calculated from the XRD spectra analysis, are reported in Table 1, which also shows the trend for the hardness and bulk modulus. It is remarkable to observe that the film with the highest T_C correspond to the film with the lower hardness and modulus.

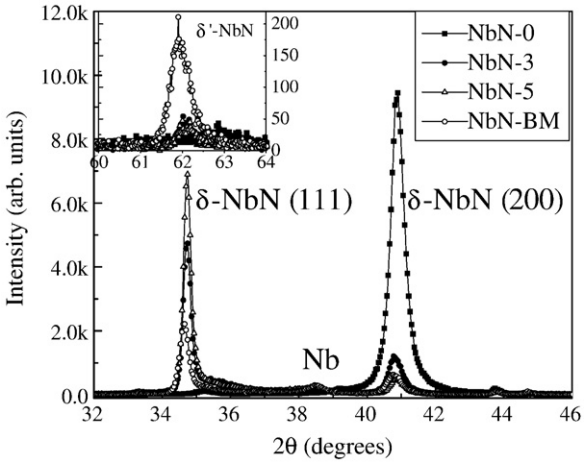

Fig. 2. X-ray diffraction patterns for the NbN films deposited with the balanced and unbalanced magnetron.

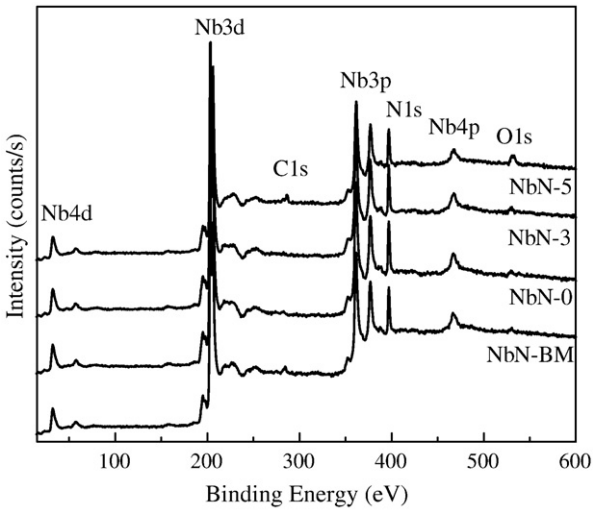

Fig. 3. XPS spectra for the NbN films deposited with both the BM and UBM magnetrons.

In order to examine the stoichiometry as well as the formation of some other phases, we analyzed the NbN films by X-ray photoelectron spectroscopy (XPS). Fig. 3 shows the XPS spectra for the NbN films deposited with both the BM and UBM magnetrons.

The chemical analysis performed by XPS showed that the Nb/N ratio was equal to 1±0.1 for all values of K. The oxygen and carbon contamination was easily removed after 3min of Ar+cleaning and thus only small signals are seen in some of the spectra, which might be an indication of the presence of NbO_x phases. Nevertheless, not chemical shift was detected among the different samples, as observed in Fig. 4(a)

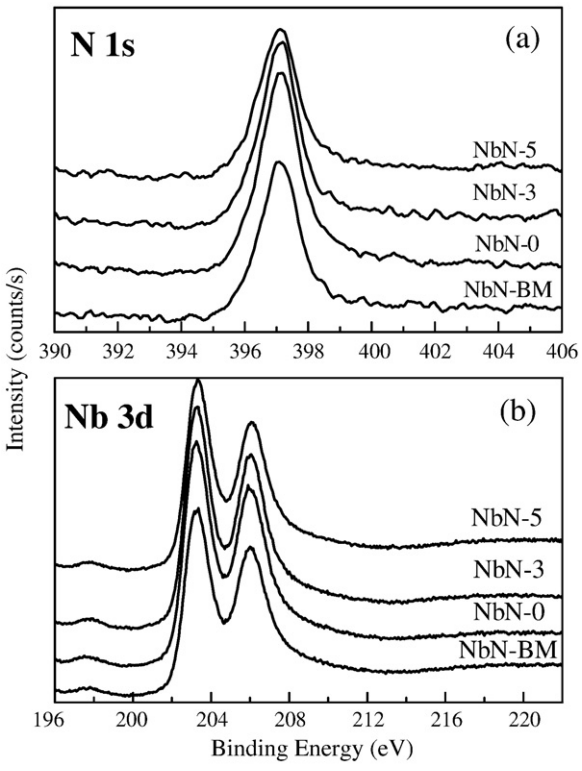

Fig. 4. (a) XPS spectra N 1s and (b) Nb 3d of NbN films deposited with both the BM and UBM magnetrons.

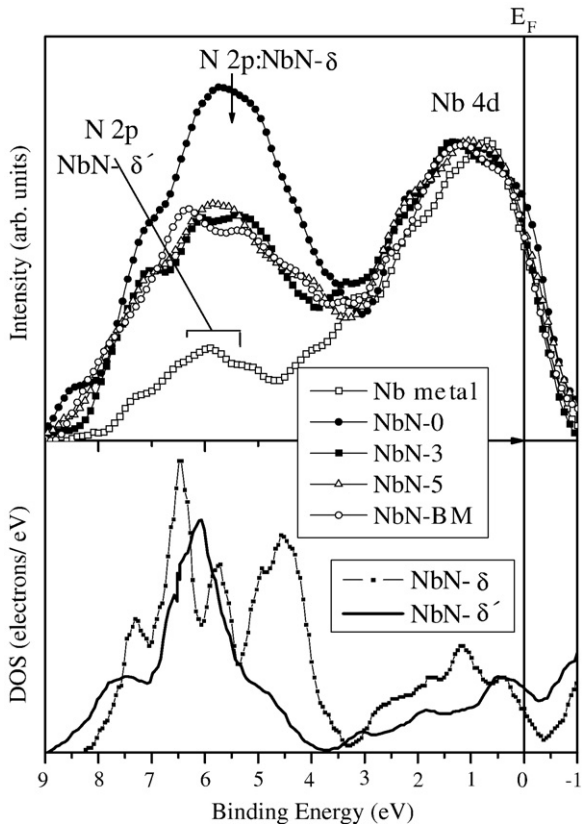

Fig. 5. Comparison of the measured valence-band spectra of NbN films deposited with both the BM and UBM magnetrons with the total density of states (DOS) of NbN calculated [36].

for the N 1s and Fig. 4(b) for the Nb 3d photoemission peaks, indicating that a similar chemical structure was predominant for all films. The high resolution spectra did not show clear contributions from the NbO_x phases. In recent papers, Lucci et al. [16,33] have shown that the highest T_C (15K) in sputtered NbN films was associated with a lower quantity of NbO_x and the right stoichiometry, and either any excess or deficiency of nitrogen induces a T_Cs around 12K.

Finally, the electronic structure was investigated by XPS high resolution spectra of the valence-band region. Fig. 5 shows the valence-band spectra of the NbN films normalized with respect to the peak near the Fermi level (E_F). It might be observed that the valence band is dominated by two peaks centered at 5.7 and 1.2eV. This is in excellent agreement with partial density of states (DOS) calculations of δ-NbN and other experimental results [34,35]. This information allow us to identify these peaks as arising from strongly hybridized N2p–Nb4d states (peak around 5.7eV), and from predominantly Nb 4d states weakly hybridized with N 2p states (peak around 1.2eV).

For comparison also the valence-band spectrum of metallic Nb sample is showed, where there are predominantly Nb 4d states and therefore the intensity of this peak decreases for the NbN samples in comparison to the high energy band due to hybridized N2p–Nb4d states. The resolution of the spectra is not so good to study the fine structure in each sample. However, it is possible to observe a splitting of the broad N 2p peak into two narrower peaks for the NbN-BM sample, which is a characteristic of the presence of the δ′-NbN hexagonal phase, as also suggested by the XRD results [34].

The other important difference observed among the films was the microstructure as can be observed in Fig. 6, where cross-section scanning electron microscopy (SEM) images of the samples deposited on silicon are shown. These images showed that the NbN-0 sample has a different microstructure; it did not show the columnar morphology as did the rest of the samples. Considering that this sample showed a very intense diffraction peak and that the cross-section morphology is clearly not columnar, it might be considered as equiaxed (zone III) according to any thin film structural zone diagram [36], meaning a more compact structure with less intergrain voids, but more evidence using transmission electron microscopy is needed to confirm this assumption.

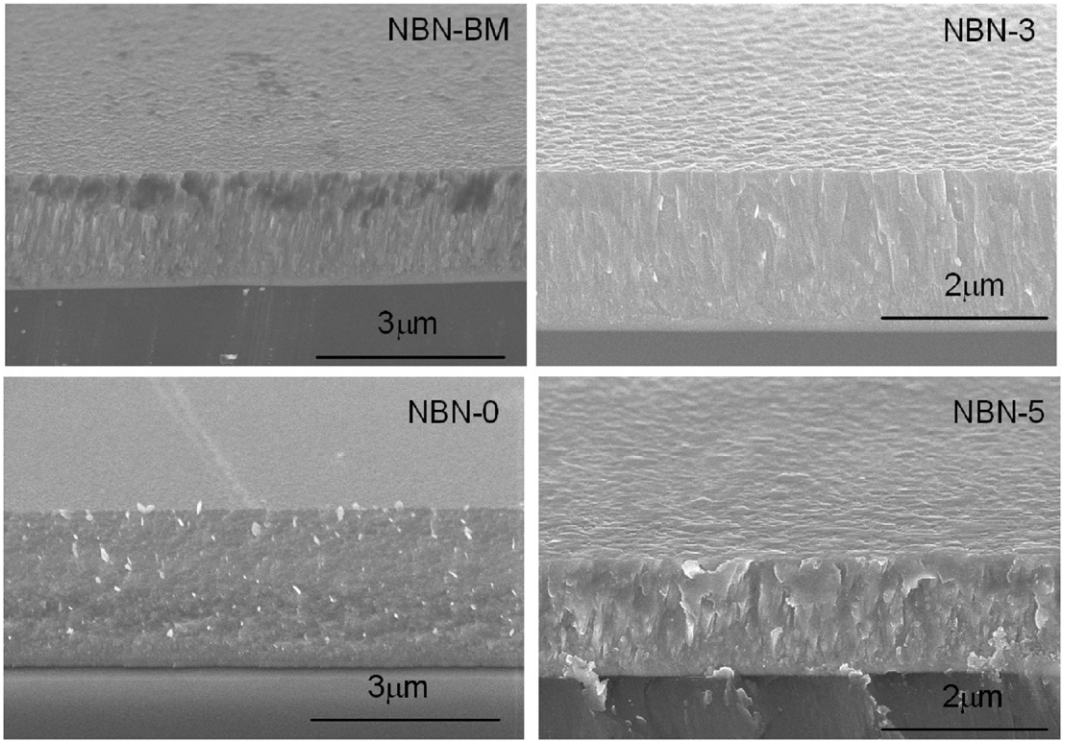

Fig. 6. Cross section SEM images of the four samples in which the different microstructures can be observed.

4. Discussion

In this work, we investigated the variations in the electrical resistance and the superconducting transition temperature of NbN thin films with the deposition conditions when using balance and unbalanced magnetron sputtering systems. We observed important differences in some sample properties, such as texture and morphology. A more detailed analysis of the explanation about the variation of the preferred orientation as a consequence of the unbalance of the magnetic field is given in Ref. [22]. Briefly, we concluded that the variation in the preferred orientation in the films can be described by a combination of two established models: the surface-strain energy model [36,37], which predicts growth along the [111] orientation for thick films and the effect of the N_2^+ dissociation due to a small increase in the ion energy (20eV), which promotes growth in the [100] direction [38,39].

Particularly interest in this paper was to understand the interrelationship between deposition conditions, microstructure, the electronic properties and the T_C value.

From the temperature dependence of the electrical resistivity of the NbN films, we could observe a variation in the temperature coefficient of resistivity from positive to negative. According to the model of Reiss et al. [40] and experimental data from other authors [41,42] these variations in the electronic transport for fully crystalline samples can be attributed to the influence of grain-boundary scattering process. The model of Reiss et al. [40] attributes the reduced resistivity of the granular media to the number density and the quantum transparency of the grain boundaries crossed by an electron during two successive scattering events. According to this model a transition from positive to negative TCR might occur for certain relation between the average grain size (D), the innercrystalline mean free path (l) and the mean probability for electrons to pass a grain boundary (Γ). Non-metallic behavior occurs when the condition $l > \frac{D}{-\ln\Gamma}$ is satisfied suggesting that this condition was satisfied for the NbN-5 sample. From the data in Table 1, we can observe that the grain sizes ranged between 13 to 35nm and no clear correlation between grain size and the sign of the TCR can be established. However, observing the cross-section SEM images, we observed that the sample with the more closed and compact microstructure, i.e., reduced grain boundaries, is the only one with a negative TCR and also the higher T_C value. According to Lucci et al. [33] only when the resistivity versus temperature curve shows a negative slope, it is possible to get a high T_C for niobium nitride films and therefore the slope of the resistivity can be considered as a good parameter of the film quality for superconductivity properties. However, in other works [24], the non-metallic conduction shape of the r vs. T curve was only associated to the grain boundary and point defect scattering effects.

The superconductivity in polycrystalline NbN films, as in many granular superconductors, has been modeled as an array of Josephson-coupled superconducting grains [43,44]. Abeles [43] showed that for granular superconductors with grain sizes between 20 and 100nm, the coupling between the grains showed superconducting properties when the junction resistance was very low. For materials with high normal resistivity, such a low values of the junction resistance could only be obtained in inhomogeneous structures where the superconductivity is due to channels formed by grains in intimate electrical contact and that the T_C vanished when there are no continuous superconducting channels. More sophisticated models [45,46] have been proposed since then, but for our purpose it is important to notice that there is a strong influence of the microstructure on the superconducting properties of granular films that can explain the different T_C values obtained for these nearly stoichiometric NbN films. Moreover, the effect of the granularity is so strong that Lamura et al. [47] have shown that by changing the texture and granularity of NbN films similar T_Cs can be obtained, but a gapless superconducting state was found for the (111)-texture films, while epitaxial or (100) textured films exhibited a characteristic superconducting gap with s-symmetry, as predicted by BCS theory. In our films, the influence of the deposition conditions and therefore of the microstructure and composition on the critical temperature can be observed in the inset of Fig. 1, where the transition to the superconducting state can be seen for three of the four films. There are differences not only on the transition temperature but also on the transition width. There is a very sharp transition for the NbN-0 sample having the higher T_C and the other two samples present a smother transition. This variation in the superconducting transition width and critical temperature might be a consequence of the different intergranular matrix properties and/or the loss of the continuous superconducting channels. Evidence for this can be observed in the SEM images.

The effect of finite grain size on the superconductive transition temperature of materials is still controversial [48], the results indicated either enhancement or loss of the superconductivity as the grain size is reduced. From the data in Table 1 it might be seen that the NbN samples evaluated have a nanocrystalline structure having grain sizes between 13 and 35nm and the highest T_C values correspond to the samples having larger grains (NbN-0 and NbN-3). However, it is clear that grain size is not the only determinant parameter since superconductive temperatures for NbN single crystals have been reported between 12.4 and 12.6K [49] while higher values have been obtained for polycrystalline NbN samples.

It is well known that changes in the T_C can also be explained as due to modifications on both the phonon spectrum and the density of states of the material [50]. This information is not easily attained, but some evidence of the variations in the density of states of the NbN films are shown in Fig. 5, where it might be seen that the sample with the highest T_C corresponds to the sample with a higher density of N2p electrons, NbN-0.

Concerning the role played by other factors affecting the scattering in thin films, we can say that surface was not relevant since the film thickness was around 2μm; larger than the mean free path, which is in the order of nanometers. Finally, the role of the crystalline defects, such as vacancies or stoichiometry was more difficult to understand, since the XPS data did not show any significant difference in the composition or bonding among the films. On the other hand, the correlation between mechanical and conductivity properties is not so clear, as discussed below. Transition metals nitrides can exist in substoichiometric phases with a substantial amount of vacancies [51,52]. Non-metal deficiency is known to be a major source of the non-stoichiometry and is crucial to the design of hard materials based on these compounds. It is expected that the vacancies reduced the number of chemical bonds and hence the strength of the materials. Experimentally, the hardness and the elastic module of group IVb nitrides such as TiN_x, ZrN_x, and HfN_x decrease as the concentration of the non-metal vacancy increases [51,53], although some contrary evidence has also been shown [54]. In our case the sample that showed the lower hardness (22GPa) was the NbN-0 sample, suggesting that it might contain a larger number of non-metal vacancies compared to the other samples. But in the other hand, the NbN-0 sample also presented the higher T_C value and according to Storms et al. [55] both metal and non-metal vacancies are effective in reducing T_C in NbN films. Moreover, from the valence-band spectra, one can observe that the intensity of the N2p signal is higher for the NbN-0 sample compared to the others. Therefore the lower hardness of this film does not seem to be associated to nitrogen vacancies, since this would also induce a decrease in the superconductive temperature and the valence-band N2p signal, contrary to the observed experimentally. One possible explanation is that the high hardness in the other films is due to a higher residual tensile stress [56], data which agrees well with the residual stress reported by J. J. Olaya [21], where it was demonstrated that the NbN-0 sample presented the lower tensile residual stress. The stress measurements were done using the Stoney's equation for thinner films deposited on silicon substrate, therefore it

does not correspond exactly to the same samples, but the general trend observed was an increment of stress as the K value increased. There is also a clear indication of residual stress in the samples in the lattice parameter reported in Table 1. The mean lattice parameter of stoichiometric FCC NbN is 4.393nm [30] and the values for all samples are higher and indeed increased as a function of the K parameter. However, it is not clear for us how the lower stress in the NbN-0 sample favors the transition to the superconductive state at higher temperature.

The lower T_C obtained for the other UBM samples could be a consequence of the smaller grain size, but most probably it is associated to the columnar void structure, as observed in the SEM images. The intercolumnar region might allocated oxygen contaminants (notice the spurious O1s signal in the XPS spectra of the NbN-5 sample), and as mentioned before the coupling between the superconducting grains might be loss. On the other hand, the NbN-BM sample presented the lower transition temperature despite that the room temperature resistivity, RRR value, grain size and hardness were not so different to that of the other samples. Therefore, we associated the low T_C value to scattering processes induced by the less ordered structure and the existence of a secondary crystalline phase, as confirmed by the XRD data and the valence-band spectra.

5. Conclusions

In this research, we have shown that by using unbalanced magnetron sputtering, it is possible to control the properties and microstructure of niobium nitride thin films. We were able to grow hard stoichiometric nanocrystalline NbN films with a superconductive transition temperature of 16K, close to the bulk value. The results from the conductivity measurements indicated that unbalanced magnetron is superior to balanced magnetron, leading in the different magnetron configurations (K from 6.5 to 9.1) to critical transition temperatures above 12K, while non superconductive transition was observed for the sample deposited in the balanced magnetron. Analyzing the structural and electrical characterization results, we can suggest that there are some correlations between the film microstructure and the T_C, but the data collected in this work is not enough to draw general conclusions.

Acknowledgements

The present work was supported by DGAPA-UNAM (Project numbers IN100701, IN100203, IX108004 & IX105404). The SEM analysis was carried out in the Center for Microanalysis of Materials, University of Illinois, which is partially supported by the U. S. Department of Energy under grant DEFG02-91-ER45439.

References

[1] A. Rando, C. Peacock, A.V. Foden, J. Dordrecht, C. Lumley, C. Pereira, J. Appl. Phys. 73 (1993) 5096.
[2] G.N. Goltsman, A.D. Semenov, Y.P. Gousev, M.A. Zorin, I.G. Gogidze, E.M. Gershenzon, P.T. Lang, W.J. Knott, K.F. Renk, Supercond. Sci. Technol. 4 (1991) 453.
[3] M. Dietrich, IEEE Trans. Magn. 21 (1985) 455.
[4] V.E. Shaternik, S.Y. Larkin, T.A. Khachaturova, Physica C 435 (2006) 96.
[5] N. Larsson, P. Hollman, P. Hendequist, S. Hogmark, U. Wahlstrom, L. Hultman, Surf. Coat. Technol. 86–87 (1996) 351.
[6] R.A. Andrievski, T.A. Anisimova, V.P. Anisimov, Thin Solid Films 205 (1991) 171.
[7] L.E. Toth, Transition Metal Carbides and Nitrides,, Academic Press, New York NY, 1971.
[8] A. Hotovy, D. Buc, J. Brcka, R. Srnanek, Phys. Stat. Solidi 161 (1997) 97.
[9] K.S. Havey, J.S. Zabinsky, S.D. Walck, Thin Solid Films 303 (1997) 238.
[10] K. Buttig, H. Liemersdorf, H. Kinder, K. Reichelt, J. Appl. Phys. 44 (1973) 5069.
[11] J. Hao, F. Jiao, D. Xie, K. Zhao, Physica C 450 (2006) 101.
[12] I. Semenov, P. Haas, K. Ill, in, H.W. Hubers, M. Siegel, A. Engel, A. Smirnov, Physica C 460–462 (2007) 1491.
[13] J.R. Gao, M. Hajenius, F.D. Tichelaar, T.M. Klapwijk, B. Voronov, E. Grishin, G. Goltsman, Appl. Phys. Lett. 91 (2007) 062504.
[14] O. Bourgeois, E. André, C. Macovei, J. Chaussy, Rev. Sci. Instrum. 77 (2006) 126108.
[15] P. Alén, M. Ritala, K. Arstila, J. Keinone, M. Lesuela, Thin Solid Films 491 (2005) 235.
[16] M. Lucci, S. Sanna, G. Contini, N. Zema, V. Merlo, M. Salvato, H.N. Thanh, I. Davoli, Surf. Sci. 601 (2007) 2647.
[17] P.J. Kelly, R.D. Arnell, Vacuum 56 (2000) 159.
[18] P.J. Kelly, R.D. Arnell, Surf. Coat. Technol. 97 (1997) 595.
[19] S.E. Rodil, J.J. Olaya, J. Phys. Condens. Mat. 18 (2006) 703.
[20] I.V. Svadkovski, D.A. Golosov, S.M. Zavatskiy, Vacuum 68 (2003) 283.
[21] S.E. Rodil, J.J. Olaya, S. Muhl, B. Bhushan, G. Wei, Surf. Coat. Technol. 201 (2007) 6117.
[22] J.J. Olaya, S.E. Rodil, S. Muhl, Thin Solid Films, In Press.
[23] L.E. Toth, Transition Metal Carbides and Nitrides, Academic Press, New York, 1971.
[24] R. Sanjinés, M. Benkahoul, C.S. Sandu, P.E. Schmid, F. Lévy, Thin Solid Films 494 (2006) 190.
[25] E.J. Cukauskas, S.B. Qadri, W.L. Carter, J. Appl. Phys. 65 (1989) 2053.
[26] M.J. Deen, D. Landheer, J.D. Wade, G.I. Sproule, M.D. Denhof, J. Vac. Sci. Technol. A 6 (1988) 2299.
[27] S. Thakoor, J.L. Lamb, A.P. Thakoor, S.K. Khanna, J. Appl. Phys. 58 (1985) 4643.
[28] T. Sahara, K. Hirao, Y. Miyamoto, M. Koizumi, J. Soc. Mater. Sci. Jpn. 37 (1988) 55.
[29] D.R. Lide, CRC Handbook of Chemistry and Physics, 82nd ed., CRC Press LLC, 2001–2002, p. 12.
[30] International Centre for Diffraction Data, Join Committee on Powder Diffraction Standards (JCPDS) database. Cards No. 171-0162 and 35-0789.
[31] L. Cunha, M. Andritschky, Surf. Coat. Technol. 111 (1999) 158.
[32] M. Fenker, M. Balzer, R.V. Buchi, H.A. Jehn, H. Kappl, J.J. Lee, Surf. Coat. Technol. 163–164 (2003) 169.
[33] M. Lucci, H. Thanh, I. Davoli, Superlattices Microstruct. 43 (2008) 518.
[34] R. Sanjines, M. Benkahoul, M. Papagno, F. Lévy, J. Appl. Phys. 99 (2006) 044911.
[35] G. Aeppli, H.J. Stolz, R.A. Pollack, Phys. Rev. B 24 (1981) 4128.
[36] I. Petrov, P.B. Barna, L. Hultman, J.E. Greene, J. Vac. Sci. Technol. A 21 (2003) S117.
[37] D. Gall, S. Kodambaka, M.A. Wall, I. Petrov, J.E. Greene, J. Appl. Phys. 93 (2003) 9086.
[38] J. Pelleg, L.Z. Zevin, S. Lungo, Thin Solid Films 197 (1991) 117.
[39] J.P. Zhao, X. Wang, Z.Y. Chen, S.Q. Yang, T.S. Shi, X.H. Liu, J. Phys. D: Appl. Phys. 30 (1997) 5.
[40] G. Reiss, J. Vancea, H. Hoffmann, Phys. Rev. Lett. 56 (1986) 2100.
[41] A. Nigro, G. Nobile, M.G. Rubino, R. Vaglio, Phys. Rev. B 37 (1988) 3970.
[42] J.H. Tyan, J.T. Lue, J. Appl. Phys. 75 (1994) 325.
[43] B. Abeles, Phys. Rev. B 15 (1977) 2828.
[44] H. Kim, K.E. Gray, R.T. Kampwirth, K.C. Woo, D.M. Kay, J. Stein, Phys. Rev. B 41 (1990) 11642.
[45] J.R. Clem, B. Bumble, S.I. Raider, W.J. Gallagher, Y.C. Shih, Phys. Rev. B 35 (1987) 6637.
[46] K. Senapati, N.K. Pandey, R. Nagar, R.C. Budhani, Phys. Rev. B 74 (2006) 104514.
[47] G. Lamura, J.C. Villegier, A. Gauzzi, J. Le Cochec, J.Y. Laval, B. Placais, N. Hadacek, J. Bok, Phys. Rev. B 65 (2002) 104507.
[48] S. Bose, R. Banerjee, A. Genc, P. Raychaudhuri, H.L. Frase, P. Ayyub, J. Phys. Condens. Mat. 18 (2006) 4553.
[49] X.J. Chen, V.V. Struzhkin, Z. Wu, R.E. Cohen, S. Kung, H.K. Mao, R.J. Hemley, A.N. Christensen, Phys. Rev. B 72 (2005) 094514.
[50] C. Phillips, J. Appl. Phys. 43 (1972) 3560.
[51] H. Holleck, J. Vac. Sci. Technol. A 4 (1986) 2661.
[52] W.S. Williams, Mater. Sci. Eng. A 105/106 (1988) 1.
[53] X. Jiang, M. Wang, K. Schmidt, E. Dunlop, J. Haupt, W. Gissler, J. Appl. Phys. 69 (1991) 3053.
[54] P. Panjan, B. Navinšek, A. Žabkar, V. Marinković, Dj Mandrino, J. Fišer, Thin Solid Films 228 (1993) 233.
[55] K. Storms, A.L. Giorgi, E.G. Szklarz, J. Phys. Chem. Solids 36 (1975) 689.
[56] S. Veprek, M.G.J. Veprek-Heijman, P. Karvankova, J. Prochazka, Thin Solid Films 476 (2005) 1.